Multimaterial 3-D Printed Compressed Luneburg Lens for mm-Wave Beam Steering

Henry Giddens, Andre Saker Andy, *Member, IEEE*, and Yang Hao, *Fellow, IEEE*

***Abstract*—Conformal, steerable lens antennas are of particular interest for millimeter-wave (mm-wave) antenna designers, as they enable low cost solutions for applications such as 5G mobile communications, radio-wave imaging, and satellite communications. Recent advances in additive manufacturing technology have opened up new possibilities for realizing graded-dielectric electromagnetic devices. In this letter, a compressed Luneburg lens fabricated from multimaterial 3-D printing is presented. Such a device has a steep dielectric gradient and cannot be easily realized using an effective medium approach that has become typical of 3-D printed graded-index devices. Instead, five different dielectric filaments were used to print the lens with a 100% filament fill-factor. The lens is excited by a WR-10 open-ended waveguide probe across the 75–110 GHz band, and achieves a bore sight gain of 22 dBi, and −3 dBi scan angle of 25° at 84 GHz.**

***Index Terms*—Lens antennas, Luneburg lens, millimeter-wave technology, multimaterial 3-D printing.**

I. Introduction

THE development of fifth generation (5G) communications has fuelled a significant interest in identifying new solutions for conformal beam steerable antennas at millimeter-wave (mm-wave) frequencies. Such antennas must radiate directive beams toward mobile users and have the ability to track multiple targets [1]. Early 5G mm-wave systems have utilized fully integrated phased arrays with either digital, analog, or hybrid beamforming networks for direct control of the antenna's radiation pattern. An alternative and often cheaper approach is the use of all-dielectric lens antennas with specific permittivity profiles designed for controlling the beam direction [2]–[9]. Antenna lens design is one area that has benefited significantly from transformation optics (TO) research, which demonstrated how electromagnetic devices can be transformed into new physical shapes without adversely affecting their performance. Practically, this means that compact devices with attractive properties can be realized. In many cases such lenses can be constructed from all-dielectric isotropic materials, removing the need for metamaterials which limit the operational bandwidth and can introduce conductive losses at higher frequencies [10].

Additive manufacturing has already evolved to a state, where it can be exploited by high-tech industries for rapid prototyping and even full-scale manufacturing. Recent advances in 3-D printed antennas have included the realization of gradient-index electromagnetic devices with increasing complexity and detail for applications spanning microwaves to terahertz [3]–[8], [11]. The permittivity variation of these devices is generally achieved by controlling the ratio of material to free space in a metamaterial/unit cell configuration [3]–[6]. The interest in 3-D printing from the electromagnetics community has fueled the development of new filament materials for specialized applications, including high-dielectric constant filaments [12]–[15] with permittivities up to a value of $\varepsilon_r = 12$. Filaments doped with magnetic materials have also been exploited in antenna applications [16].

The Luneburg lens is able to focus a plane wave incident onto any of its surfaces to a point on the opposite surface. In antenna engineering, these devices have seen significant development due to the advances additive manufacturing techniques and the wide scope of potential applications requiring low-cost beam steering solutions for which they are suited. Examples include Luneburg lenses which follow the traditional material profile, where there is no impact on beam steering degradation but the lens forms a spherical or cylindrical shape [17]–[20], and transformed versions of the lens, which trade beam steering performance at wide angles for a more conformal aperture or planar feed arrays [5], [9], [21]–[28].

In this letter, we present the fabrication and performance of a compressed Luneburg lens at 75–110 GHz fabricated through multimaterial fused deposition modeling (FDM) 3-D printing with five different dielectric filaments. The compressed Luneburg lens is particularly suited to multimaterial printing as the permittivity gradient from the center of the lens to its surface is steep, varying from $\varepsilon_r = 7.5$ to $\varepsilon_r = 3$ over a distance of just 3.8 mm. Such a gradient would be extremely difficult to achieve using a single material and the effective medium approach, as it would require a printer with ultra-fine resolution in order to create a small unit cell with dimensions. Finally, metamaterial-based lenses require optimized unit-cell design in order to achieve the required effective permittivities of different regions of the lens while maintaining structural integrity and wideband performance. Multimaterial 3-D printing therefore offers a low-cost solution to these problems. The lens presented in this work radiates with a gain of 21 ± 1 dBi over the 75–110 GHz frequency bands, and the measured radiation patterns of the lens has a boresight gain of 22 dBi, and beam steering performance of $\pm 25°$ with only 3 dBi reduction in peak gain. The advantages of this solution compared to traditional Luneburg lens structures are

Manuscript received July 9, 2021; revised August 13, 2021; accepted August 16, 2021. Date of publication September 2, 2021; date of current version November 16, 2021. This work was supported by the EPSRC Projects AOTOMAT EP/P005578/1, ANIMATE EP/R035393/1, and SYMETA EP/N010493/1. *(Corresponding author: Henry Giddens.)*

The authors are with the School of Electronic Engineering and Computer Science, Queen Mary University London, E1 4NS London, U.K. (e-mail: h.giddens@qmul.ac.uk; a.andy@qmul.ac.uk; y.hao@qmul.ac.uk).

Digital Object Identifier 10.1109/LAWP.2021.3109591

the low profile and slim aperture, simple manufacturing process, and planar beam steering capability, while it also maintains high gain across the 70–110 GHz band.

II. Compressed Luneburg Lens

The Luneburg lens is a spherical lens with a spatially varying refractive index that has a value of $\sqrt{2}$ in the center and 1 on its surface [2]. The Luneburg lens is able to focus light propagating as a plane wave into a single point located on the diametric opposite surface of the lens to the direction of propagation. Due to the large volume and low dielectric constant required to realize the devices, spherical Luneburg lenses have not often been utilized by antenna engineers at low microwave and radio-frequency applications. However, with the emergence of TOs, such lenses have become particularly relevant at higher microwave and millimeter wave frequencies, as conformal beam-steerable lenses can be excited from different points, generating multiple beams in different directions.

For example, transforming the curved surface of the Luneburg lens onto a flat aperture allows for beam steering to be achieved by moving the source across a single plane. Such transformations can be achieved by moving the focal point to the center of the lens, as proposed by Gutman in 1954 [25], [29] or by using quasi-conformal coordinate mapping technique [3], [23]. A completely flat Luneburg lens transformation, where the spherical shape is transformed onto cylindrical boundaries, has also been fabricated and experimentally verified using dielectrically loaded ceramics cast into cylindrical moulds [26]. Quevedo-Teruel and Hao [24] showed how the Luneburg lens could be transformed into various diffused shapes while maintaining directive and steerable radiation.

An alternative coordinate transformation of the Luneburg lens has also been proposed, known as the compressed Luneburg lens [9], [22]. The compressed Luneburg lens is essentially squashed along one of its axes, resulting in a steep dielectric gradient profile, while maintaining the ability to steer the beam generated from a point source. Numerical studies have shown that beam-steering of up to $\pm 25^\circ$ can be achieved with less than 3 dB reduction in the peak directivity.

The refractive index profile of the spherical Luneburg lens can be calculated by (1), where R is the total lens radius, and r is the radial position inside the lens

$$n = \sqrt{\varepsilon} = \sqrt{2 - \left(\frac{r}{R}\right)^2}. \tag{1}$$

The lens can be compressed along the x-axis by a compression factor δ, by following the coordinate transform in (2) and (3). The material properties required in the transformed coordinate system, represented by x' and y', can easily be calculated by (4) and (5) [9], [22]

$$x' = \frac{x}{\delta} \tag{2}$$

$$y' = y \tag{3}$$

$$\varepsilon' = \varepsilon \begin{pmatrix} \delta & 0 \\ 0 & 1/\delta \end{pmatrix} = \left(2 - \frac{y'^2 + \delta x'^2}{R^2}\right) \begin{pmatrix} \delta & 0 \\ 0 & 1/\delta \end{pmatrix} \tag{4}$$

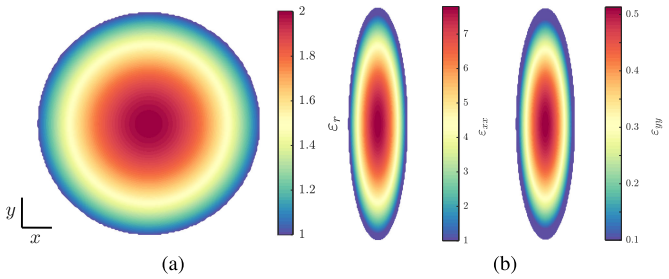

Fig. 1. Permittivity map of (a) the original Luneburg lens. (b) ε'_{xx} component of the compressed Luneburg lens. (c) ε'_{yy} Component of the compressed lens. The compression factor δ is equal to 3.9.

$$\mu = \begin{pmatrix} \delta & 0 \\ 0 & 1/\delta \end{pmatrix}. \tag{5}$$

The permittivity map of the compressed Luneburg lens with $\delta = 3.9$ can be viewed in Fig. 1. It should be noted that (2) to (5) produce a value of ε'_{yy} less than 1. Previous studies have shown that the compressed lens can make the assumption that $\varepsilon'_{yy} = 1$, to avoid the use of dispersive metamaterials, without any significant impact on performance. It can also be assumed that $\mu = 1$ to avoid the inclusion of magnetic materials [9], [22], [24].

III. Lens Fabrication

Lens antennas are typically electrically large as they are utilized to produce directive beams. FDM 3-D printing is particularly suited to fabricating models with a physical size in the range of tens of millimeters to tens of centimeters, due to the tradeoff between printing time, physical feature resolution, material cost, and scalability. In terms of electrically large antennas, 3-D printing is therefore probably most suited to fabricating devices operating in the mm-wave bands. We therefore designed the compressed Luneburg lens to operate at 84 GHz. The initial Luneburg lens (before compression) had an outer radius of 13.5 mm. The compressed lens was discus shaped and had an x-radius of 4 mm on its outer surface and y-radius of 14 mm.

The permittivity gradient along the x-axis and the y- and z-axes is displayed in Fig. 2. In the center of the lens, the permittivity is at a maximum of 7.8. The permittivity reduces to a value of 1 on the surface of the lens over a distance of just 4 mm in the x-axis. In y- and z-axes, the permittivity values change across the same total range, however at a total distance of 4.1 mm. A total of five different dielectric ABS filaments were selected for printing the lens [13] with permittivity values ranging from 3 to 7.5. For each filament, four samples were printed with 100% fill factor for characterization of their dielectric properties at 75–110 GHz. The samples were characterized using quasi-optical transmission measurements, where permittivity and loss were retrieved via the Nicholson–Ross Weir method. The measured relative permittivity and loss tangent data are shown in Fig. 3 as an average of the four printed samples. At 84 GHz, the filament permittivities were 3, 4.5, 5.5, 6.5, and 7.5, with loss remaining below 0.02 throughout the frequency band.

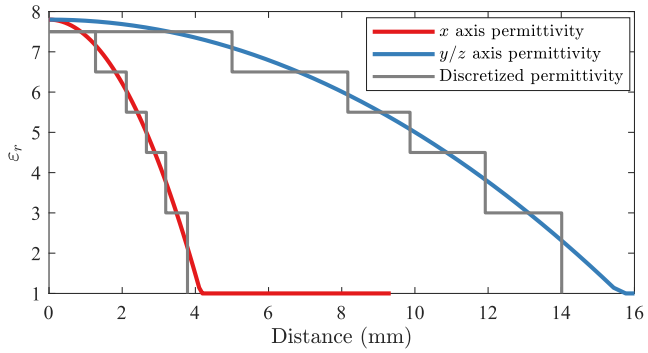

Fig. 2. Permittivity gradient of the compressed lens along the x-axis and the y- and z-axes. The permittivity gradient is steep in both directions and would not be feasible using an effective medium approach that is often associated with 3-D printed dielectric antennas. The straight lines show the average permittivity gradient for a specific section of the lens and therefore show the radial dimensions and permittivity values of the discretized lens.

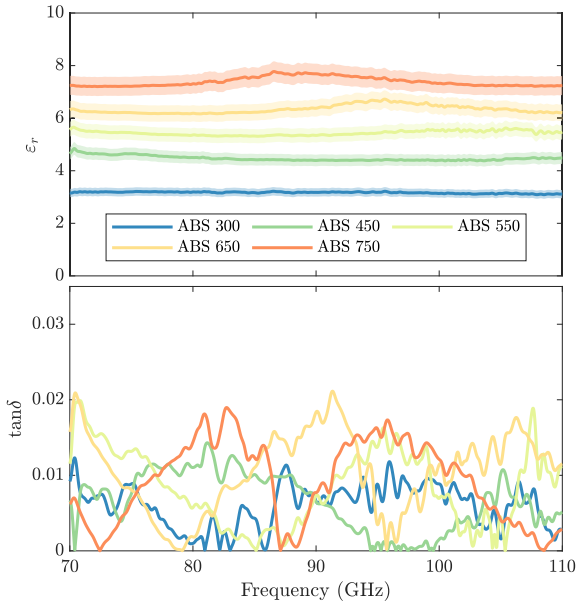

Fig. 3. Measured dielectric properties of filaments used in the lens fabrication from [13].

The lens was discretized into five different sections, where the average permittivity values were equivalent to the materials available. The boundaries of the discretized permittivity regions are also shown in Fig. 2. Such a steep permittivity gradient, especially in the x-axis, is not particularly feasible to fabricate using single-material 3-D printing and the metamaterial approach, due to the limitations of 3-D printed antennas previously discussed. The lens was printed using a Prusa i3 MK3S/MMU2S 3-D printer, which has the capability to print with up to five different materials in a single print. Using a single nozzle, different materials are loaded and unloaded from the hot end in sequence until each material required for a single layer has been extruded. When a new material is loaded into the nozzle, a fixed amount of filament is extruded onto a purge tower in order to ensure that any old filament left in the hot end has been removed and does not then get printed into the model. In order to maintain the same curvature profile on the front and back of the lens, the model was

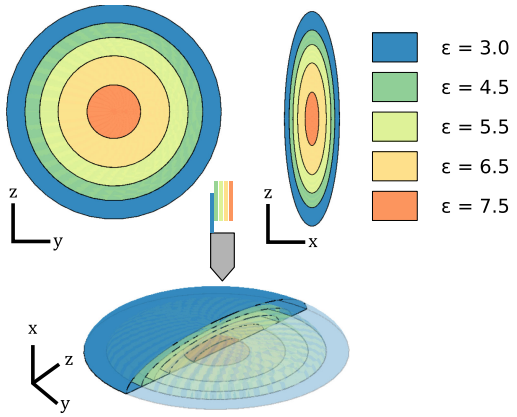

Fig. 4. Top: Cross-sectional view of the different parts of the compressed Luneburg lens for 3-D printing. Bottom: Perspective view of the compressed lens orientated in the position that it was 3-D printed.

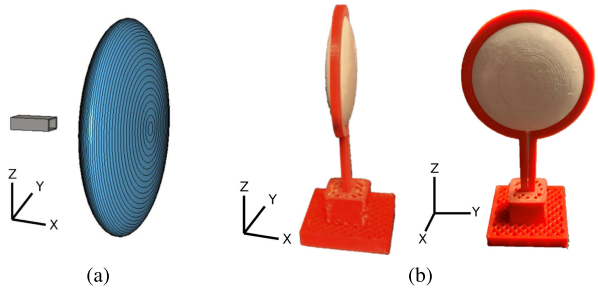

Fig. 5. (a) Computer-aided design (CAD) model of the compressed lens with open-ended waveguide feed. (b) Photographs of the 3-D printed lens.

sliced in half along the yz-plane. Fig. 4 shows the cross sections of the lens and illustrates how it was printed. In order to orientate the lens correctly for 3-D printing, the half-lens was laid flat on the print bed, with the smaller radial length orientated along the vertical axis of the printer. The two halves of the lens were hot pressed together and no additional adhesive was used. They were further held in place with the 3-D printed lens holder. The lens was printed with a layer height of 0.1 mm. The total print time for a single lens was 3 h 15 m. However, most of the time is taken in the filament loading procedure. Fabricating multiple lenses in a single print would be more time efficient as it would not result in a linear increase in the total print time. The fabricated lens is shown in Fig. 5.

IV. Lens Characterization

The lens was excited with a WR-10 open-ended waveguide with dimensions of 2.54 $\times$ 1.27 mm. The focal distance was determined by moving the waveguide to the point at which the gain of the lens was at a maximum [9], and was located at a distance of 7.2 mm. The gain of the WR-10 probe with and without the lens was measured by comparing the magnitude of the transmitted power to that of a WR-10 27240-20 standard gain horn antenna and is displayed in Fig. 6. At 84 GHz, the probe alone has a gain of 7.3 dBi, which increased to 22.1 dBi with the introduction of the lens. Over the 75–100 GHz frequency band, the gain remained stable at 21 $\pm$1 dBi, confirming its wideband

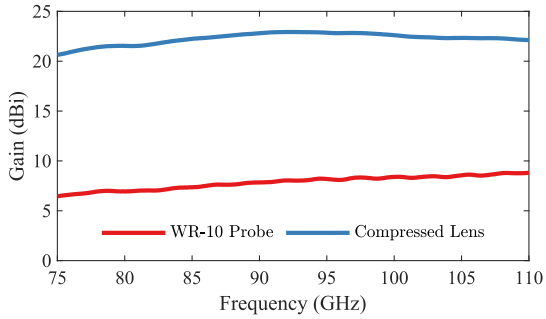

Fig. 6. Measured gain of WR-10 open-ended waveguide probe and the 3-D printed compressed lens.

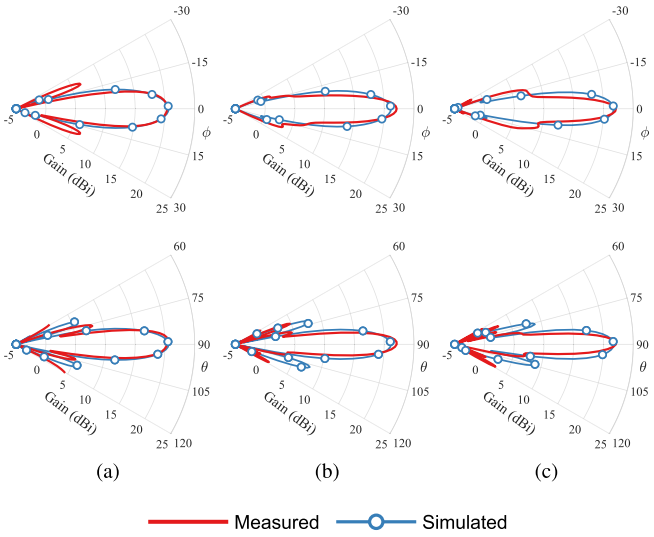

Fig. 7. *H*-plane (top) and *E*-plane (bottom) radiation patterns of the 3-D printed compressed Luneburg lens antenna measured at (a) 75, (b) 84, and (c) 105 GHz.

radiation characteristics. A slight drop in gain at the higher end of the band due to less effective illumination of the lens as the feed becomes more directive.

The performance of the compressed Luneburg lens was simulated using CST Microwave Studio. The dielectric materials forming the lens were modeled with the permittivity values shown in Fig. 3 and loss tangent of 0.01 [13]. The radiation patterns were measured at 75, 84, and 105 GHz using a planar near-field scanner and performing a near-to-far transformation. The simulated reflection coefficient was matched to below -9 dB across the entire band, as expected from an open-ended waveguide. Fig. 7 displays the boresight *E*- and *H*-plane radiation patterns from measurements and simulations with the probe positioned in the center of the *y*- and *z*-axes at these frequencies. As can be seen, the pattern shapes agree well. At the center frequency of 84 GHz, the lens radiates with no sidelobes in the $\pm 30^\circ$ angular span. Sidelobes are slightly higher at the lower end of the band, appearing at $\pm 25^\circ$ with a magnitude of 14 dBi below the peak. The directivity of the lens at 84 GHz was 24.3 dBi. When compared with the gain of 22.1 dBi, there is a difference of 2.3 dB, leading to a total antenna efficiency of 60%. This is in line with the simulated data which calculated an efficiency of 70%, the difference due to manufacturing tolerances.

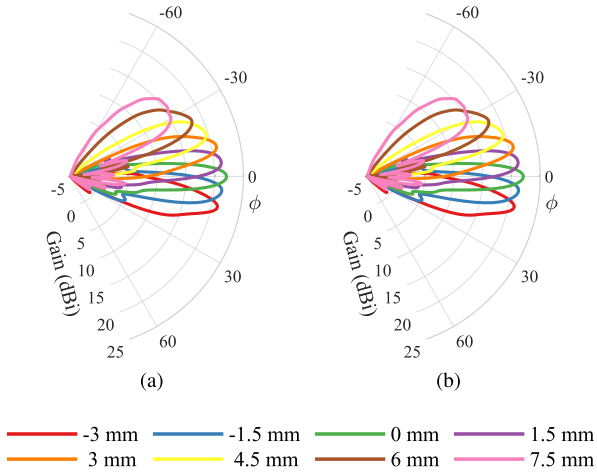

Fig. 8. Measured beam-steering performance of the lens in (a) the *H*-plane and (b) the *E*-plane at 84 GHz. The legend shows to the displacement distance of the WR-10 probe along (a) *y*-axis and (b) the *z*-axis.

Fig. 8 shows the measured *H*- and *E*-plane beam steering performance. In order to achieve the beam steering, the probe was displaced in the *yz*-plane behind the lens by steps of 1.5 mm. As can be seen, Luneburg lens enables beam steering in both planes, maintaining a well-defined main beam. In the *H*-plane, the maximum gain of the lens falls to 19 dBi at an angle of 25° with a *y*-axis displacement of 6 mm. The beam can be steered further, to an angle of 35°, albeit with a reduction in gain down to 16 dBi, by moving the feed to a displacement of 7.5 mm. The *E*-plane steering experiences a larger initial scan-loss, the maximum beam falling to 17 dBi with a 4.5 mm offset at a steering angle of 20°, although the signal strength is maintained up to a steering angle of 30° with 6 mm offset. The difference in the *E*- and *H*-plane steering performance is due to different levels of illumination efficiency from the feeding antenna. The scan loss of the lens is around $\cos(1.4\theta)$ and is therefore higher than a typical planar phased array, which experiences a $\cos\theta$ gain reduction with steering angle. However, the lens still provides good steering performance between $\pm$ 30° and has advantages in terms of cost, simplicity, and wideband performance.

V. Conclusion

In this letter, a 3-D printed, multimaterial, compressed Luneburg lens has been presented. The compressed lens was designed through a simple coordinate transformation of the original Luneburg lens in order to reduce its width by a factor of 3.8. Due to the steep permittivity gradient required from the compressed lens, multimaterial 3-D printing was used to manufacture the lens. The fabricated lens radiated with a realized gain of 21 $\pm$1 dBi over the 75–110 GHz frequency band. The measured radiation patterns at 84 GHz showed beam steering performance of 25° with a 6 mm displacement of the feed position. Conformal, low cost, and high-performance antennas operating in the mm-wave bands, such as the compressed Luneburg lens presented here, will be important in realizing commercially viable mm-wave systems in consumer devices for 5G networks.

REFERENCES

[1] D. Muirhead, M. A. Imran, and K. Arshad, "A survey of the challenges, opportunities and use of multiple antennas in current and future 5G small cell base stations," *IEEE Access*, vol. 4, pp. 2952–2964, 2016.

[2] R. K. Luneburg, *Mathematical Theory of Optics*. Providence, RI, USA: Brown Univ. Press, 1944, pp. 189–213.

[3] H. Feng Ma and T. Jun Cui, "Three-dimensional broadband and broad-angle transformation-optics lens," *Nature Commun.*, vol. 1, no. 1, pp. 1–7, Nov. 2010.

[4] M. Liang, W. Ng, K. Chang, K. Gbele, M. E. Gehm, and H. Xin, "A 3D Luneburg lens antenna fabricated by polymer jetting rapid prototyping," *IEEE Trans. Antennas Propag.*, vol. 62, no. 4, pp. 1799–1807, Apr. 2014.

[5] Z. Larimore, S. Jensen, A. Good, A. Lu, J. Suarez, and M. Mirotznik, "Additive manufacturing of Luneburg lens antennas using space-filling curves and fused filament fabrication," *IEEE Trans. Antennas Propag.*, vol. 66, no. 6, pp. 2818–2827, Jun. 2018.

[6] Z. Larimore, S. Jensen, P. Parsons, B. Good, K. Smith, and M. Mirotznik, "Use of space-filling curves for additive manufacturing of three dimensionally varying graded dielectric structures using fused deposition modeling," *Additive Manuf.*, vol. 15, pp. 48–56, 2017.

[7] F. Zhou, W. Cao, B. Dong, T. Reissman, W. Zhang, and C. Sun, "Additive manufacturing of a 3D terahertz gradient-refractive index lens," *Adv. Opt. Mater.*, vol. 4, no. 7, pp. 1034–1040, 2016.

[8] D. Isakov, C. J. Stevens, F. Castles, and P. S. Grant, "3D-Printed high dielectric contrast gradient index flat lens for a directive antenna with reduced dimensions," *Adv. Mater. Technol.*, vol. 1, no. 6, 2016, Art. no. 1600072.

[9] A. Demetriadou and Y. Hao, "Slim Luneburg lens for antenna applications," *Opt. Exp.*, vol. 19, no. 21, pp. 19 925–19 934, Oct. 2011.

[10] O. Quevedo-Teruel *et al.*, "Transformation optics for antennas: Why limit the bandwidth with metamaterials?," *Sci. Rep.*, vol. 3, 2013, Art. no. 1903.

[11] R. Yang, W. Tang, and Y. Hao, "A broadband zone plate lens from transformation optics," *Opt. Exp.*, vol. 19, no. 13, pp. 12 348–12 355, Jun. 2011.

[12] F. Castles *et al.*, "Microwave dielectric characterisation of 3D-printed $BaTiO_3$/ABS polymer composites," *Sci. Rep.*, vol. 6, Mar. 2016, Art. no. 22714.

[13] "PREPERM filaments for 3D printing," Accessed: Jan. 11, 2019. [Online]. Available: https://web.archive.org/web/20190111123238/https://www.preperm.com/products/stock-shapes/

[14] H. Kim, J. Johnson, L. A. Chavez, C. A. G. Rosales, T.-L. B. Tseng, and Y. Lin, "Enhanced dielectric properties of three phase dielectric MWCNTs/$BaTiO_3$/PVDF nanocomposites for energy storage using fused deposition modeling 3D printing," *Ceramics Int.*, vol. 44, no. 8, pp. 9037–9044, 2018.

[15] U. Kalsoom, P. Nesterenko, and B. Paull, "Recent developments in 3D printable composite materials," *RSC Adv.*, vol. 6, vol. 65, pp. 60355–60371, Jan. 2016.

[16] J. Sorocki, I. Piekarz, I. Slomian, S. Gruszczynski, and K. Wincza, "Realization of compact patch antennas on magneto-dielectric substrate using 3D printing technology with iron-enhanced PLA filament," in *Proc. Int. Conf. Electromagn. Adv. Appl.*, Sep. 2018, pp. 185–188.

[17] Q. Liao, N. J. G. Fonseca, and O. Quevedo-Teruel, "Compact multibeam fully metallic geodesic Luneburg lens antenna based on non-Euclidean transformation optics," *IEEE Trans. Antennas Propag.*, vol. 66, no. 12, pp. 7383–7388, Dec. 2018.

[18] B. Qu, S. Yan, A. Zhang, F. Wang, and Z. Xu, "3D printed cylindrical Luneburg lens for dual polarization," *IEEE Antennas Wireless Propag. Lett.*, vol. 20, no. 6, pp. 878–882, Jun. 2021.

[19] S. Lei, K. Han, X. Li, and G. Wei, "A design of broadband 3D-printed circularly polarized spherical Luneburg lens antenna for X-band," *IEEE Antennas Wireless Propag. Lett.*, vol. 20, no. 4, pp. 528–532, Apr. 2021.

[20] M. Mirmozafari, M. Tursunniyaz, H. Luyen, J. H. Booske, and N. Behdad, "A multi-beam tapered cylindrical Luneburg lens," *IEEE Trans. Antennas Propag.*, vol. 69, no. 8, pp. 5060–5065, Aug. 2021.

[21] Y. Li, L. Ge, M. Chen, Z. Zhang, Z. Li, and J. Wang, "Multibeam 3D-printed Luneburg lens fed by magnetoelectric dipole antennas for millimeter-wave MIMO applications," *IEEE Trans. Antennas Propag.*, vol. 67, no. 5, pp. 2923–2933, May 2019.

[22] A. Demetriadou and Y. Hao, "A grounded slim Luneburg lens antenna based on transformation electromagnetics," *IEEE Antennas Wireless Propag. Lett.*, vol. 10, pp. 1590–1593, 2011.

[23] Y. Li and Q. Zhu, "Luneburg lens with extended flat focal surface for electronic scan applications," *Opt. Exp.*, vol. 24, no. 7, pp. 7201–7211, Apr. 2016.

[24] O. Quevedo-Teruel and Y. Hao, "Directive radiation from a diffuse Luneburg lens," *Opt. Lett.*, vol. 38, no. 4, pp. 392–394, Feb. 2013.

[25] O. Quevedo-Teruel, W. Tang, and Y. Hao, "Isotropic and nondispersive planar fed Luneburg lens from Hamiltonian transformation optics," *Opt. Lett.*, vol. 37, no. 23, pp. 4850–4852, Dec. 2012.

[26] C. Mateo-Segura, A. Dyke, H. Dyke, S. Haq, and Y. Hao, "Flat Luneburg lens via transformation optics for directive antenna applications," *IEEE Trans. Antennas Propag.*, vol. 62, no. 4, pp. 1945–1953, Apr. 2014.

[27] C. Wang, Y. Xia, G. Guo, M. Nasir, and Q. Zhu, "Ellipsoidal Luneburg lens binary array for wide-angle scanning," *IEEE Trans. Antennas Propag.*, vol. 68, no. 7, pp. 5702–5707, Jul. 2020.

[28] Y. Su and Z. N. Chen, "A radial transformation-optics mapping for flat ultra-wide-angle dual-polarized stacked GRIN MTM Luneburg lens antenna," *IEEE Trans. Antennas Propag.*, vol. 67, no. 5, pp. 2961–2970, May 2019.

[29] A. S. Gutman, "Modified Luneberg lens," *J. Appl. Phys.*, vol. 25, pp. 855–859, Jul. 1954.